Chemical Physics Letters 635 (2015) 185–189

Contents lists available at ScienceDirect

Chemical Physics Letters

journal homepage: www.elsevier.com/locate/cplett

Carbon nanotubes decorated by mesoporous cobalt oxide as electrode material for lithium-ion batteries

K. Wenelska[a,*], C. Neef[b], L. Schlestein[b], R. Klingeler[b,c], Ryszard J. Kalenczuk[a], E. Mijowska[a]

[a] Institute of Chemical and Environment Engineering, West Pomeranian University of Technology, ul. Pulaskiego 10, 70-322 Szczecin, Poland
[b] Kirchhoff Institute for Physics, Heidelberg University, INF 227, 69120 Heidelberg, Germany
[c] Centre for Advanced Materials, Heidelberg University, INF 225, 69120 Heidelberg, Germany

ARTICLE INFO

Article history:
Received 10 March 2015
In final form 25 June 2015
Available online 6 July 2015

ABSTRACT

We report a facile strategy to synthesize carbon nanotubes decorated by mesoporous cobalt oxide (CNT@Co_3O_4). The mesoporous nature of the nanocomposite is confirmed by transmission electron microscopy, scanning electron microscopy, and X-ray diffraction. The data imply 41 wt% mesoporous Co_3O_4 spheres in the as-prepared material with mean diameters ~12 nm. The nanospheres are embedded in an interconnected network of carbon nanotubes. The specific surface area of CNT@Co_3O_4 amounts to 463 m^2/g. Cyclic voltammetry studies show a high activity of the Co^{2+}/Co^0 and Co^{3+}/Co^{2+} redox couples. The conversion reaction is observed and full theoretical capacity is found in the 2nd cycle while significant capacity fading appears upon further cycling. Decorating mesoporous metal oxide nanospheres onto the interconnected electrically conducting network of carbon nanotubes therefore provides a first step towards an electrochemically active material promising for lithium-ion batteries.

1. Introduction

Nanoarchitectures have been shown to be of great relevance in catalysis [1], electrocatalysis [2], and as electrodes in energy storage devices [3,4]. Reducing the size of primary particles in materials to nanodimensions typically leads to larger electrode/electrolyte interface areas and shorter diffusion lengths. In addition, new intrinsic properties related to particular nanomorphologies can be generated. This approach of downscaling bulk materials towards nanostructured architectures has offered a route to design cutting-edge materials with improved performance, particularly in the major field of lithium-ion (Li-ion) rechargeable batteries [5–9]. Li-ion batteries are the most developed energy storage technology for mobile applications because of their attractive high gravimetric and volumetric energy densities. However, since the initial commercial introduction of Li ion batteries composed of $LiCoO_2$ and graphite as cathode and anode materials, respectively, development of lithium ion batteries has fallen behind the rise in demand for safer, higher energy density and longer life cycle batteries [5,10]. Owing to their high theoretical electrochemical capacities associated with conversion reactions, which are much higher than in graphite, transition-metal oxide nanoparticles (MO-NPs with M = Co, Ni, Cu or Fe) are particularly promising anode materials [11–13]. However, large volume expansion upon Li insertion/extraction destabilizes the structure of the MO and derogates the electrical contacts within the materials and towards the current collector, resulting in poor cyclability and rate capabilities. Despite diverse attempts to overcome these drawbacks, including the development of nano- and microstructured carbon-based composites such as nano-SnO_2/carbon [14], MoO_2/CNT [15], Mn_3O_4/graphene [16] or nano-Fe_3O_4/carbon composites [17], there is still a high demand to substantially improve the electrochemical performance of potential anode materials for usage in Li-ion batteries.

Due to the conversion reaction, Co_3O_4 can in principle accommodate eight lithium ions per formula unit and is hence one of the most promising anode materials which might replace graphitic carbon [5]. However, practical application of Co_3O_4 has been frustrated due to the abovementioned issues, i.e. large volume changes upon (de)lithiation and particle aggregation, which leads to electrode pulverization, capacity loss and poor cycling stability [18]. To overcome these limitations and to enhance the electrochemical performance, Co_3O_4 may be combined with carbon materials, such as CNTs. Due to high chemical stability, high electrical conductivity, large accessible surface area, and facile functionalization,

* Corresponding author.
E-mail address: kwenelska@zut.edu.pl (K. Wenelska).

http://dx.doi.org/10.1016/j.cplett.2015.06.072
0009-2614/

carbon nanotubes (CNTs) are attractive electrode materials in electrochemical energy storage devices themselves [19–23]. CNTs have unique morphological characteristics: in addition to the high surface area it is the extremely high aspect ratio which efficiently can generate interconnected networks of percolating CNT. The pore structure of CNTs increases the contact area with the electrolyte, thereby improving the electrochemical performance of CNT-based materials [24] in contrast to some other carbon materials, such as activated carbons [25,26]. This has been shown for several MO. MnO/CNT composites has generated a substantial increase in performance [27] as well as exohedral functionalization of CNTs by Mn_3O_4 [24]. Even filling of CNTs is a potential route as shown by Yan et al. in the case of Fe_2O_3 nanoparticles [28]. Previous work in the literature however shows, that simple and effective ways have still to be developed in order to synthesize larger quantities of such nanostructures for actual applications.

In this work, we report a facile strategy to synthesize carbon nanotubes decorated by mesoporous cobalt oxide, i.e. CNT@Co_3O_4. The porous structure of cobalt oxide is expected to facilitate the diffusion of electrolyte into the electrode material and to provide more channels for rapid ion transport. The material is thoroughly characterized by means of TEM, SEM, XRD, Raman spectroscopy, and the surface area and pore size distribution are determined. Cyclic voltammetry (CV) was carried out to evaluate the electrochemical characteristics and to obtain initial information on the capacity of CNT@Co_3O_4.

2. Experimental

2.1. Synthesis of CNT@Co_3O_4

In a typical preparation procedure, 100 mg of CNTs (carbon nanotubes, multi-walled ≥98% carbon basis, Sigma–Aldrich) were suspended in 30 ml deionized water and 30 ml ethylene glycol and sonicated for 1 h. Subsequently, 250 mg of cobalt acetate tetrahydrate (Sigma–Aldrich) was added to the mixture and the reaction mixture was refluxed for 48 h at 110 °C. The reactant was filtered through a 0.4 μm PTFE membrane filter, washed extensively with water to remove of ethylene glycol. Finally, the resulting carbon nanotubes decorated by mesoporous cobalt oxide nanoparticles (CNT@Co_3O_4) were dried at 100 °C in air for 24 h.

2.2. Methodology

X-ray diffraction (XRD) was conducted on a Philips diffractometer using Cu-K_α radiation. The morphology of the samples was examined by a FEI Tecnai F30 transmission electron microscope (TEM) with a field emission gun operating at 200 kV. To examine the dimensions and the particles' shape of the material, a Scanning Electron Microscope (SEM) Zeiss, Leo1530 was used. N_2 adsorption/desorption isotherms were acquired at liquid nitrogen temperature (77 K) using a Micromeritics ASAP 2010 M instrument, and the specific surface area was calculated by the Brunauer–Emmett–Teller (BET) method. The pore size distribution was determined using the Barret–Joner–Halenda (BJH) method. Raman scattering was conducted on a Renishaw micro-Raman spectrometer (λ = 720 nm). Thermogravimetric analysis (TGA) was carried out on 10 mg samples using the DTA-Q600 SDT TA at a heating rate of 10 °C/min from room temperature to 900 °C under air.

2.3. Electrochemical measurements

Electrochemical measurements were carried out using Swagelok-type cells [29]. The working electrodes were prepared by mixing the samples CNT@Co_3O_4, carbon black (Timcal), and polyvinyl difluoride (PVDF) (Solvay Plastics) at a weight ratio of 80:10:10, respectively, and pasting the slurry onto Cu foils (diameter ~10 mm) with a typical load of 4 mg/cm^2. A lithium foil was used as counter electrode and 1 M $LiPF_6$ solution in a 1:1 EC/DMC mixture (Sigma–Aldrich) was used as electrolyte. The cells were assembled in an Ar-filled glovebox with less than 1 ppm moisture and oxygen. Cyclic voltammetry measurements were carried out by using a VMP3 multichannel potentiostat (BIO-Logic SAS, France) in a climate chamber at 298 K. The scan rate was fixed at 0.05 mV/s in the voltage range of 0.01–3.00 V.

3. Results and discussion

The morphology of the CNT@Co_3O_4 nanocomposite was studied by means of TEM and SEM. Both the TEM (Figure 1a–c) and the SEM (Figure 1d and e) images show the composite nature of the resulting nanomaterials. As seen in Figure 1a–e, there are porous cobalt oxide nanoparticles interconnected by CNT. A detailed analysis reveals very uniform diameters of the CNT of ~10 nm as well as a particle size distribution of the cobalt oxide spheres with diameters between 100 and 250 nm (Figure 1f).

Figure 2 shows the Raman spectra of the CNT@Co_3O_4 nanocomposite, which confirm the composition of the material. Firstly, there are two broad peaks at 1310 and 1596 cm^{-1}, which are fingerprints of the carbon material, i.e. the D-band and G-band, respectively. The G-band is associated with the vibrational modes of the sp^2-bonded carbon atoms in a graphitic layer, whereas the D-band indicates the presence of defects in the graphene lattice [30]. The additional peaks at 187, 472, and 678 cm^{-1} correspond to vibrational modes of Co_3O_4 [31,32]. Therefore, the Raman response of the sample confirms the presence of the spinel Co_3O_4 phase.

Figure 3 shows the typical X-ray diffraction (XRD) pattern of the as-prepared CNT@Co_3O_4 nanocomposite material. All diffraction peaks showing up in Figure 3 either refer to face-centred cubic Co_3O_4 or are associated with the CNT present in the material. To be specific, diffraction peaks at 2θ = ~19°, 31°, 37°, 38°, 56°, 59°, and 65° (labelled by filled circles) match well with that of face-centred cubic Co_3O_4. There are additional relatively broad diffraction peaks appearing at 2θ = 24° and 45° (labelled by filled squares) which are due to the crystalline carbon of the CNTs. The absence of any other diffraction peaks excludes the presence of significant impurity phases. The rather large width of the diffraction peaks indicates the small size of the Co_3O_4 nanoparticles. According to Scherrer's equation, $D_{XRD} = 0.89\lambda/(\Delta \cos \Theta)$, the crystallite size of the nanoparticles can be calculated from the full width at half maximum Δ of the diffraction peak corresponding to the Bragg angle Θ [33]. Taking into account the (3 1 1), (4 4 0), and (5 1 1) diffraction peaks, the analysis yields a mean diameter of $D_{XRD} = 12 \pm 1$ nm, which nicely agrees to the results of the TEM analysis in Figure 1f.

Thermogravimetric analysis (TGA) of pristine CNT and CNT@Co_3O_4 has been performed in air atmosphere (see Figure 4). The carbon nanotubes begin to decompose at 552 °C in air. As the temperature is further increased, the weight loss increases rapidly until all of the carbon nanotubes are exhausted at about 610 °C. TGA of sample does not have ashes after the burning procedure indicating high purity of the sample. TGA of CNT@Co_3O_4 shows that most of the carbon skeleton starts to burn at temperatures above 470 °C. It suggests that the CNT after cobalt oxide deposition is more defected and start to decompose at lower temperature than pristine CNT. Upon further heating above ~600 °C, there are no significant weight changes which suggests complete oxidation of carbon. From the ash content of CNT@Co_3O_4 after combustion we hence conclude an amount of 41 wt% mesoporous cobalt oxide spheres in the as-prepared material.

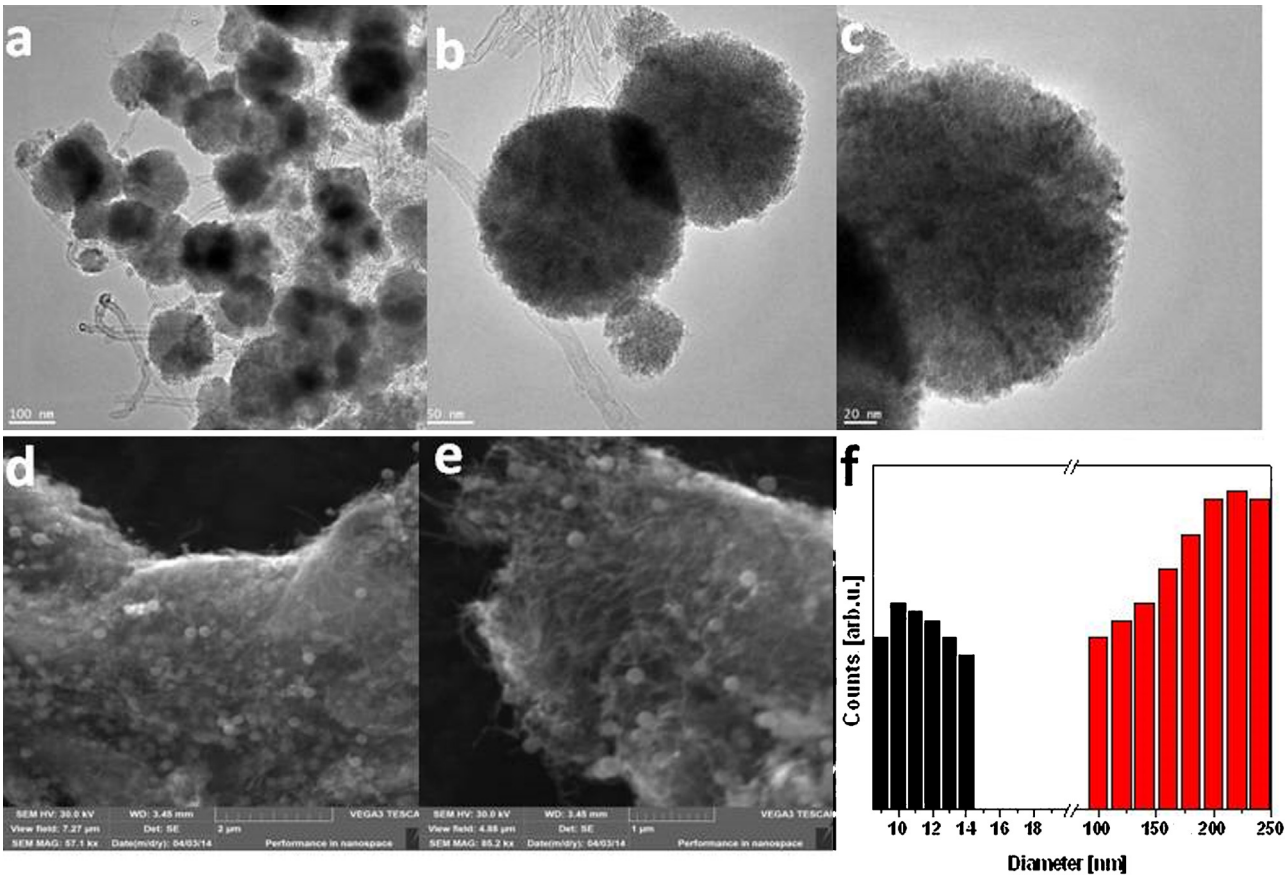

Figure 1. TEM (a–c) and SEM (d and e) images of carbon nanotubes decorated by mesoporous cobalt oxide spheres. (f) Diameter distribution of the carbon nanotubes and mesoporous cobalt oxide, respectively.

The specific surface area of the CNT@Co_3O_4 was studied by the BET method. Nitrogen isotherms presented in Figure 5a show a typical type II behaviour with a H1 hysteresis loop, indicating a disordered mesoporous structure in the CNT@Co_3O_4 nanocomposite. The BET specific surface area for the material amounts to 463 m^2/g. The corresponding mesopore size distribution calculated by means of the BJH method from the adsorption branch reveals non-uniform pores centred at approximately 3.4, 4,5, 6.7, 8.4, 11, 17 and 23 nm, as shown Figure 5b. This result implies a mesoporous structure of the Co_3O_4 spheres present in the material.

The electrochemical behaviour of the CNT@Co_3O_4 nanocomposite is visible in Figure 6 which displays CV curves in the potential range between 0.01 V and 3 V recorded at a scan rate of 0.05 mV/s. The first cycle is characterized by a strong and irreversible cathodic peak at 0.75 V, which can be attributed to both the formation of a passivating solid–electrolyte-interface (SEI) layer accompanied by electrolyte decomposition [34] and the initial reduction process of Co_3O_4 to metallic cobalt and formation of amorphous Li_2O.

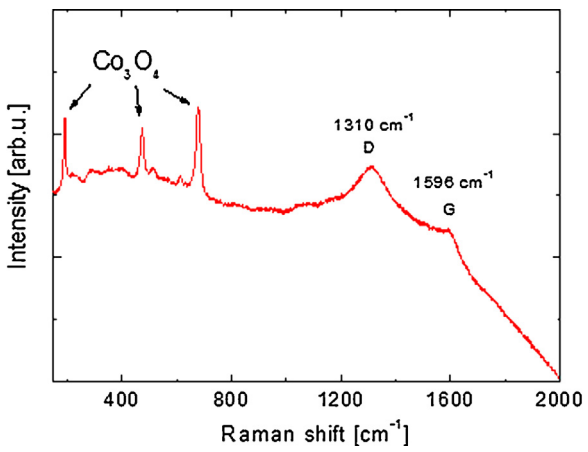

Figure 2. Raman spectroscopy of the CNT@Co_3O_4 nanocomposite.

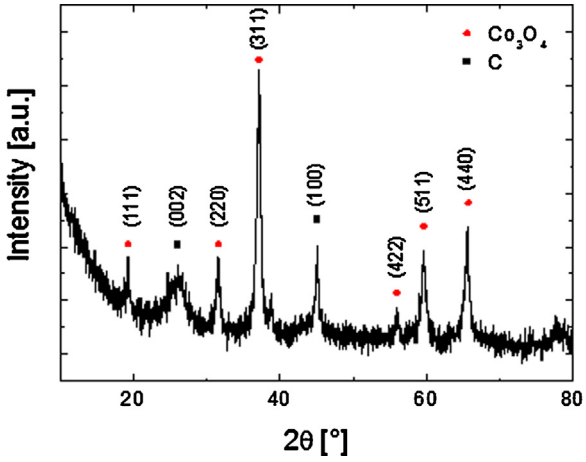

Figure 3. XRD pattern of the CNT@Co_3O_4 nanocomposite material.

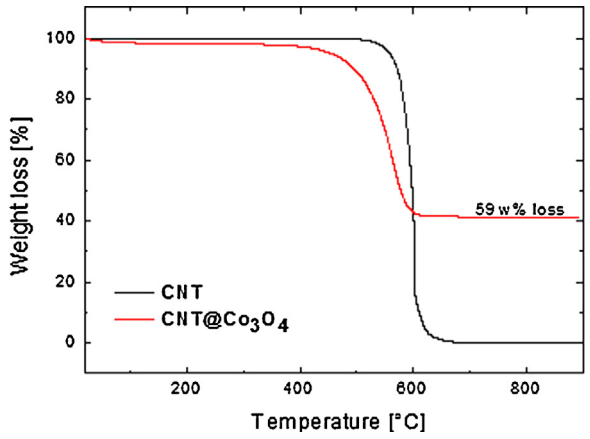

Figure 4. TGA profile of pristine CNT and CNT@Co_3O_4 nanocomposite.

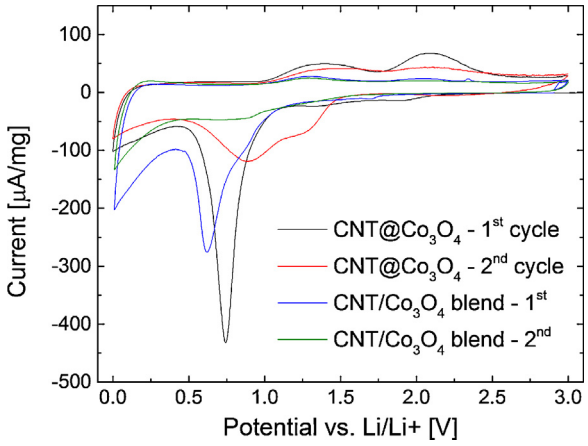

Figure 6. Cyclic voltammogram (CV) curves of the CNT@Co_3O_4 nanocomposite in first (black) and second (red) cycle. For comparison, the 1st and 2nd cycle of a post-synthesis mixture of Co_3O_4 and CNTs is shown, too (blue, green). (For interpretation of the references to color in this figure legend, the reader is referred to the web version of the article.)

The anodic scan and following cycles exhibit an oxidative double peak with maxima located at 1.4 V and 2.1 V and reductive peaks at 1.3 V and 0.9 V, respectively. These double peaks correspond to a multi-step redox reaction caused by the Co^{2+}/Co^0 and Co^{3+}/Co^{2+} couples [34,35]. Note that the regime of electrochemical activity of the CNTs is assumed to be below 0.3 V [36,37]. Clear reaction peaks might however be masked by the strong Co_3O_4 activity.

In order to further investigate the advantage of the hybrid nanomaterial at hand and to assess utilizing of hybrid nanostructures, a control experiment was carried out on a CNT/Co_3O_4 blend (see Figure 6). Here, separately fabricated CNT and Co_3O_4 nanoparticles were mechanically mixed post-synthesis in the same ratio of 59% CNT and 41% Co_3O_4 which according to TGA is realized in the decorated CNT@Co_3O_4 nanocomposite. The CVs on the blend exhibit similar peak positions. However, the peak intensities strongly decrease already in the 2nd cycle. Note, that the position of the first cathodic peak is shifted towards lower potentials for the post-synthesis blend, which might be caused by a higher over-potential due to lower conductivity of the electrode.

To investigate the lithium storage capacity of the studied materials, the integrated specific capacities were calculated from the CVs (see Figure 7). For data analysis, the actual active material's composition was used including additional 10% of carbon black added during electrode preparation. The full theoretical capacity for this composition is calculated as 560 mAh/g (dashed line in Figure 7). For calculating this value, an equivalent of 8 lithium atoms per formula unit was considered for Co_3O_4 (890 mAh/g) and 1 lithium atom per C_6-ring for CNTs and carbon black (372 mAh/g). As displayed in Figure 8, after a large initial charge capacity of 850 mAh/g observed in the 1st cycle associated with irreversible side reactions, the full theoretical capacity is observed in the second cycle.

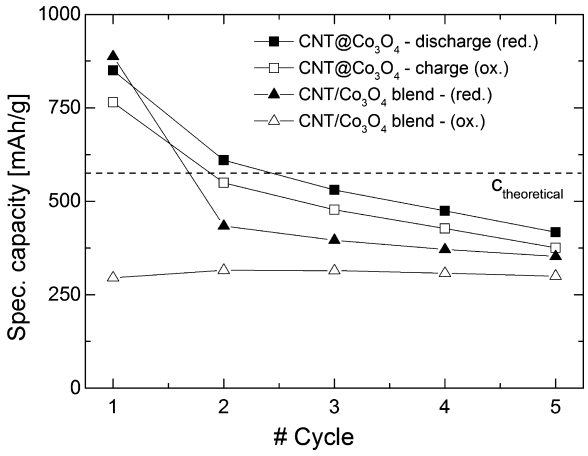

Figure 7. Integrated charge and discharge capacity for 5 cycles as deduced from CVs. The dashed line indicates the theoretical reversible capacity of the material.

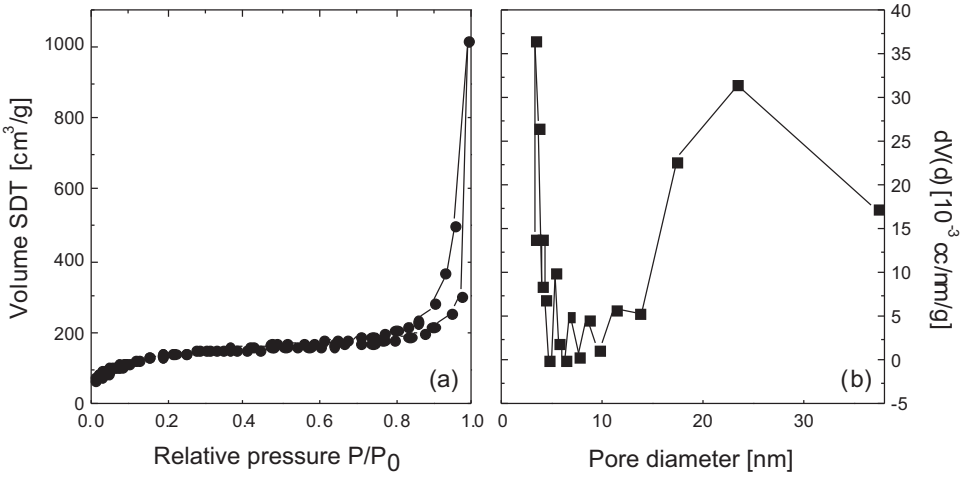

Figure 5. (a) N_2 adsorption–desorption isotherm profile and (b) pore size distribution profile of the CNT@Co_3O_4 nanocomposite.

While a similarly high reductive capacity is measured for the post-synthesis blend in the first cycle, the associated reversible capacity is much lower as compared to the CNT@Co_3O_4 hybrid nanomaterial. Furthermore the irreversible loss between charge and discharge capacity is higher.

To summarize, the electrochemical experiments show that the CNT@Co_3O_4 hybrid nanostructures offer an effectual network with good electronic conduction and electrolyte saturation. Our synthesis approach proofs to give a material with improved kinetics and higher activity as compared to the individual components. However, upon longer cycling, a capacity loss is observed, which is most likely related to irreversible changes in the electrodes structure due to the high volume change and thus mechanical stress during the lithiation reaction.

4. Conclusions

Nanocomposite CNT@Co_3O_4 consisting of carbon nanotubes decorated by mesoporous cobalt oxides were synthesized and studied regarding their potential as electrodes in Lithium ion batteries. The electrochemical studies show that the conversion reaction in the mesoporous cobalt oxide nanospheres is observed and full theoretical capacity is found in the 2nd cycle. Our results hence demonstrate high electrochemical activity of the nanocomposite while however the material has to be optimized in order to reduce capacity fading upon further cycling. Decorating mesoporous metal oxide nanospheres onto the interconnected electrically conducting network of carbon nanotubes therefore provides an electrochemically active material promising for lithium-ion batteries. The design and synthesis strategy of the material reported in this study can be used for other metal oxides as well, such as NiO, and V_2O_5, so that a large class of materials can be optimized for such application.

Acknowledgments

The authors are grateful for the financial support of National Science Centre PRELUDIUM 6 UMO-2013/11/N/ST8/00651 and SONATA BIS – UMO-2012/07/E/ST8/01702, German Academic Exchange Service DAAD (PPP Project No. 56269175), the NanoTech-Initiative of the Baden-Württemberg-Stiftung (Project Nanostorage).

References

[1] N. Brun, K. Sakaushi, J. Eckert, M.M. Titirici, ACS Sustain. Chem. Eng. 2 (2014) 126.
[2] M. Lefevre, E. Proietti, F. Jaouen, J. Dodelet, Science 324 (2009) 71.
[3] A. Arico, P. Bruce, B. Scrosati, J. Tarascon, W. Van Schalkwijk, Nat. Mater. 4 (2005) 366.
[4] L. Nazar, G. Goward, F. Leroux, M. Duncan, H. Huang, T. Kerr, J. Gaubicher, Int. J. Inorg. Mater. 3 (2001) 191.
[5] P. Poizot, S. Laruelle, S. Grugeon, L. Dupont, J. Tarascon, Nature 407 (2000) 496.
[6] P. Bruce, B. Scrosati, J. Tarascon, Angew. Chem. Int. Ed. 47 (2008) 2930.
[7] E. Hosono, T. Kudo, I. Honma, H. Matsuda, H. Zhou, Nano Lett. 9 (2009) 1045.
[8] B. Kang, G. Ceder, Nature 458 (2009) 190.
[9] M. Okubo, Y. Mizuno, H. Yamada, J. Kim, E. Hosono, H. Zhou, T. Kudo, I. Honma, ACS Nano 4 (2010) 741.
[10] W.L. Yao, J. Yang, J.L. Wang, L.A. Tao, Electrochim. Acta 53 (2008) 7326.
[11] X. Liu, C. Chen, Y.B. Zhao, J. Nanomater. 2013 (2013) 375.
[12] Z.H. Wang, L.X. Yuan, Q.G. Shao, F. Huang, Mater. Lett. 80 (2012) 110.
[13] B. Varghese, M.V. Reddy, Z. Yanwu, C.S. Lit, T.C. Hoong, G.V.S. Rao, B.V.R. Chowdari, A.T.S. Wee, C.T. Lim, C.H. Sow, Chem. Mater. 20 (2008) 3360.
[14] Z. Fu, X. Li, G. Xu, Cryst. Res. Technol. 49 (2014) 441.
[15] A. Bhaskar, M. Deepa, T.N. Rao, ACS Appl. Mater. Interfaces 5 (2013) 2555.
[16] H. Wang, J. Am. Chem. Soc. 132 (2010) 13978.
[17] Y. Chen, Adv. Funct. Mater. 24 (2014) 319.
[18] L. Wang, Y. Zheng, X. Wang, S. Chen, F. Xu, L. Zuo, J. Wu, L. Sun, Z. Li, H. Hou, Y. Song, ACS Appl. Mater. Interfaces 6 (2014) 7117.
[19] E. Frackowiak, S. Gautier, H. Gaucher, S. Bonnamy, F. Beguin, Carbon 37 (1999) 61.
[20] B. Gao, A. Kleinhammes, X.P. Tang, C. Bower, L. Fleming, Y. Wu, O. Zhou, Chem. Phys. Lett. 307 (1999) 153.
[21] S.W. Lee, N. Yabuuchi, B.M. Gallant, S. Chen, B.S. Kim, P.T. Hammond, Y. Shao-Horn, Nat. Nanotechnol. 5 (2010) 531.
[22] S. Nardecchia, D. Carriazo, M.L. Ferrer, M.C. Gutierrez, Chem. Soc. Rev. 42 (2013) 794.
[23] R.H. Baughman, A.A. Zakhidov, W.A. de Heer, Science 297 (2002) 787.
[24] Z.-H. Wang, L. Yuan, Q. Shao, F. Huang, J. Huang, Mater. Lett. 80 (2012) 110.
[25] K.H. An, W.S. Kim, Y.S. Park, Y.C. Choi, S.M. Lee, D.C. Chung, D.J. Bae, S.C. Lim, Y.H. Lee, Adv. Mater. 13 (2001) 497.
[26] E. Frackowiak, K. Metenier, V. Bertagna, F. Beguin, Appl. Phys. Lett. 77 (2000) 2421.
[27] G.L. Xu, Y.F. Xu, H. Sun, Chem. Commun. 48 (2012) 8502.
[28] N. Yan, et al., Sci. Rep. 3 (2013) 3392, http://dx.doi.org/10.1038/srep03392
[29] C. Jähne, C. Neef, C. Koo, H.-P. Meyer, R. Klingeler, J. Mater. Chem. A 1 (2013) 2856.
[30] J. Gamby, P.L. Taberna, P. Simon, J.F. Fauvarque, M.J. Chesneau, Power Sources 101 (2001) 109.
[31] A.G. Pandolfo, A.F.J. Hollenkamp, Power Sources 157 (2006) 11.
[32] J. Ren, L. Li, C. Chen, X. Chen, Z. Cai, L. Qiu, Y. Wang, X. Zhu, H. Peng, Adv. Mater. 25 (2013) 1155.
[33] Y. Huang, J. Lin, Y. Bando, C. Tang, C. Zhi, Y. Shi, E. Takayama-Muromachi, D. Golberg, J. Mater. Chem. 20 (2010) 1007.
[34] L. Zhuo, Y.Q. Wu, J. Ming, L. Wang, Y. Yu, X. Zhang, F. Zhao, J. Mater. Chem. A 1 (2013) 1141.
[35] M. Xu, F. Wang, Y. Zhang, S. Yang, M. Zhao, X. Song, Nanoscale 5 (2013) 8067.
[36] Z.-H. Yang, H.-Q. Wu, Solid State Ionics 143 (2001) 173.
[37] Z. Xiong, Y.S. Yun, H.-J. Jin, Materials 6 (2013) 1138.